Available online at www.sciencedirect.com
ScienceDirect
Trans. Nonferrous Met. Soc. China 30(2020) 647−656
Transactions of Nonferrous Metals Society of China
www.tnmsc.cn

Influence of trace Ca addition on texture and stretch formability of AM50 magnesium alloy sheet

Hong-liang ZHAO[1], Yun-xiao HUA[1], Xiang-lei DONG[1], Hui XING[2], Yan-li LU[3]

1. College of Materials Science and Engineering, Zhengzhou University, Zhengzhou 450001, China;
2. The MOE Key Laboratory of Material Physics and Chemistry under Extraordinary Conditions, Northwestern Polytechnical University, Xi'an 710129, China;
3. State Key Laboratory of Solidification Processing, Northwestern Polytechnical University, Xi'an 710072, China

Received 13 June 2019; accepted 17 December 2019

Abstract: The AM50, AM50−0.1Ca, AM50−0.3Ca and AM50−0.5Ca (wt.%) alloys were hot-rolled and their mechanical properties were determined for the purpose of investigating the effect of trace Ca addition on the texture and stretch formability of AM50 alloy. The results show that the addition of trace Ca can effectively modify the basal texture, which is characterized by the split of basal poles deviated from the normal direction (ND) after the hot rolling, while a broad spread of the basal planes toward the transverse direction (TD) after the annealing. Such change of the basal texture is related to the prior formation of massive compression twins and the decrease of the *c*/*a* ratio. Erichsen value increases from 2.25 to 4.21 mm with the increase of Ca content. The enhancement of stretch formability is ascribed to the weakened basal texture, which results in the increase of *n*-value and the decrease of *r*-value.
Key words: magnesium alloy; Ca addition; texture; stretch formability; mechanical properties

1 Introduction

Wrought magnesium alloy sheets have gained extensive attentions from the automotive industry owing to their better processing properties in comparison with those cast ones [1−3]. Compared to the traditional commercial wrought magnesium AZ31 alloys, the AM series alloy such as AM50 alloy has the unique advantages of higher strength and comparatively favorable ductility [4,5], which exhibits a promising potential for wrought magnesium materials. However, the poor stretch formability, due to the formation of strong basal texture during the deformation process has limited their further applications. Therefore, modifying the basal texture to enhance the stretch formability of the Mg alloy sheet presents great scientific and industrial significance.

Microalloying is an effective method to modify the basal texture, which can be easily achieved by adding trace amounts of alloying elements into the matrix alloys [6]. It has been reported that the trace addition of rare earth elements such as Y, Ce and Gd can effectively contribute to the weakened basal texture and thus result in the enhanced stretch formability [6−8]. But, these expensive rare earth elements substantially increase the costs of raw materials. It is, therefore, essential to find other cost-effective alternatives. Ca, as a low-cost alloying element, can not only refine the microstructure of magnesium alloy, but also has the similar effect on the texture weakening compared to rare earth elements [9−13]. However, the mechanism on the texture control is still not clear and the study on the stretch formability by

Foundation item: Projects (51801186, 51974281) supported by the National Natural Science Foundation of China; Project (SKLSP 201814) supported by the Fund of the State Key Laboratory of Solidification Processing in Northwestern Polytechnical University, China
Corresponding author: Xiang-lei DONG; Tel: +86-13460293820; E-mail: dxl881112@zzu.edu.cn
DOI: 10.1016/S1003-6326(20)65243-8

adding trace Ca individually into Mg alloys still obtains few attentions. Therefore, it can be provided an opportunity for the development of the low-cost Mg alloy sheets with Ca addition based on the AM50 alloy.

In this study, the alloys with different Ca additions have been prepared for evaluating the effect of Ca on the texture and stretch formability of AM50 alloy sheet. The microstructure evolution during the hot rolling, and the basal textures of the as-rolled and annealed alloy sheets were investigated. The corresponding mechanical properties and stretch formability were determined. This work is expected to provide the theoretical and technological guidance for the development of wrought magnesium alloy sheets in automobile industry.

2 Experimental

Experiments were started on the preparation of the investigated alloys, with the chemical compositions given in Table 1. The melting process was carried out in a crucible resistance furnace under the protective atmosphere (SF_6+CO_2) at 740 °C. Mn and Ca were added in form of Mg−15wt.%Mn and Mg−30wt.%Ca master alloys. After being completely melted, the alloys were cast into a preheated steel mold with the sizes of 150 mm × 120 mm × 9 mm. The ingots for rolling were machined into the samples with the dimensions of 80 mm × 80 mm × 8 mm and then homogenized at 420 °C for 24 h. Rolling process was carried out at 400 °C and held at this temperature for 10 min between passes, and the final thickness of the sheets was 1 mm with a total cumulative reduction of 87% over 13 passes. Finally, the rolled sheets were annealed at 350 °C for 1 h.

The metallographic samples were sectioned, cold-mounted, polished and then etched in the picric acid solution (2.1 g picric acid, 10 mL acetic acid, 10 mL distilled water, and 70 mL ethanol) for the microstructure observation on optical microscope. Electron back scattered diffraction (EBSD) analysis were performed on a Zeiss/Auriga FIB SEM machine operating at 15 kV to reveal the textures of the as-rolled and annealed alloy samples. The Ultima IV X-ray diffractometer using Cu K_α radiation was employed to measure the lattice parameters of the powder alloy samples. The tensile specimens with 1 mm in gauge thickness, 20 mm in gauge length and 10 mm in gauge width were machined from the annealed sheets with the angles of 0°, 45° and 90° between the tensile direction and the rolling direction. The Shimadzu/AG-X plus electronic universal testing machine was used for the measurement of the mechanical properties at an initial strain rate of 1×10^{-3} s^{-1} at room temperature. The strain hardening exponent values (*n*-values) were obtained by the data of tensile tests with a strain interval from 5% to 15% and the Lankford values (*r*-values) were measured on the specimens deformed at a plastic strain of 10%. The samples for Erichsen tests were machined from the annealed sheets with the dimensions of 60 mm × 60 mm × 1 mm. Erichsen tests were carried out at room temperature on the CB2−60D cup convex testing machine using a hemispherical punch with a diameter of 20 mm, the speed and the blank holder force of which were 5 mm/min and 10 kN, respectively. The Erichsen values (IE), which were the punch stroke at the fracture initiation, were directly obtained from the data acquisition system. The average values were given by averaging the IE from three repeated experiments.

Table 1 Chemical compositions of investigated alloys (wt.%)

Alloy	Al	Mn	Ca	Mg
AM50	4.94	0.32	0	Bal.
AM50−0.1Ca	5.13	0.29	0.12	Bal.
AM50−0.3Ca	5.08	0.32	0.28	Bal.
AM50−0.5Ca	4.96	0.31	0.47	Bal.

3 Results and discussion

3.1 Microstructures during hot rolling

The microstructures of the four alloy sheets on the RD−ND plane during hot rolling are shown in Fig. 1, with the cumulative total deformation of 29%, 47%, 66% and 87%. Generally, there exist two types of twins during the hot deformation: the $\{10\bar{1}2\}$ tensile twins with lenticular morphology and the $\{10\bar{1}1\}$ compression twins with narrow banded appearance [14,15]. It is observed that the tensile twins are apparent and the recrystallization has occurred in some twin regions in the early

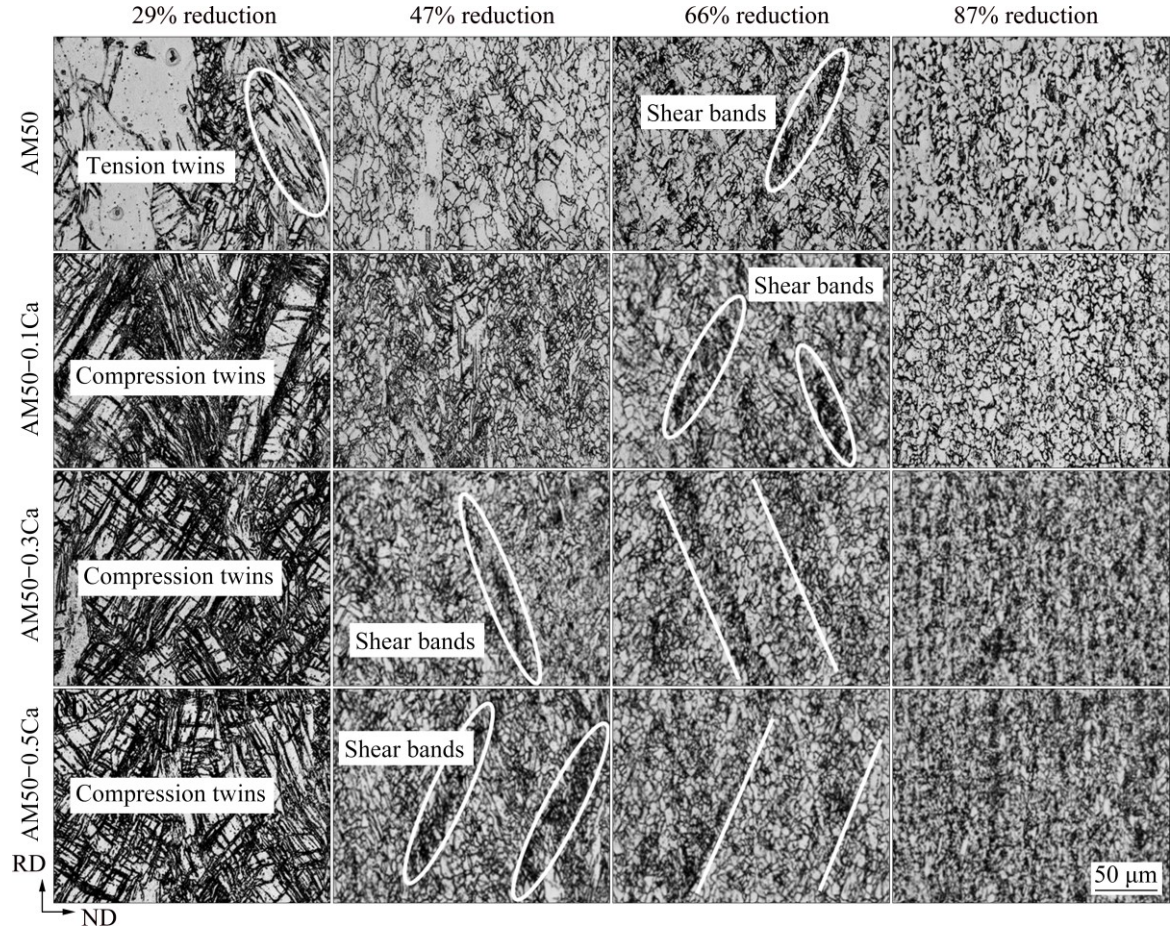

Fig. 1 Microstructures of alloys on RD−ND plane during hot rolling: (a) AM50; (b) AM50−0.1Ca; (c) AM50−0.3Ca; (d) AM50−0.5Ca

deformation stages of the AM50 alloy, but there still exist a large proportion of original grains. By comparison, massive narrow banded compression twins appear and interlace with each other in the Ca-containing alloys. Original grains are divided into many long and block regions, and few recrystallized grains can be observed in these intersection areas. With the increase of thickness reduction, the recrystallization processes occur remarkably in these alloys, showing that the deformation twins disappear, while the number of recrystallized grains increases rapidly. It is obvious that the shear bands with black stripe structures appear at the reduction of 66% in the AM50 and AM50−0.1Ca alloys, whereas the higher proportion of shear bands form at a lower reduction of 47% in the AM50−0.3Ca and AM50−0.5Ca alloys. These deformed shear bands continue to broaden in the further reductions, which gives rise to the finer and more homogeneous microstructures after the last pass rolling.

Generally, owing to the minimum critical resolved shear stress (CRSS), the $\{10\bar{1}2\}$ tensile twins are easy to occur in the initial stages of the hot deformation [16]. But, in the present study, the $\{10\bar{1}1\}$ compression twins preferentially appear during the hot rolling in Ca-containing alloys. This indicates that the addition of trace Ca has changed the twinning behavior of the AM50 alloy. The dominant mechanism of twinning is highly dependent on the stacking fault energy (SFE) [17], which is closely related to the difference of the atomic size. The greater difference between alloying elements and Mg atomic radius tends to obtain the lower SFE [18]. For example, the addition of Y element has promoted the formation of $\{10\bar{1}1\}$ compression twins and $\{10\bar{1}1\}-\{10\bar{1}2\}$ secondary twins, which was ascribed to the reduction of SFE [19]. In our study, the radii of Al and Mn atoms are both smaller than radius of Mg atom, while Ca has the atomic radius equivalent to Y, as well as the largest atomic radius difference

compared with other elements. This suggests that the addition of Ca into AM50 alloy can significantly induce the local lattice distortion and the consequent decrease of the SFE. Therefore, the prior formation of $\{10\bar{1}1\}$ compression twins after Ca addition can be attributed to the decrease of the SFE.

The shear bands are apparent with various proportions at different reductions, which is related to the formation of different types of deformation twins. Compared to the tensile twins, the massive compression twins in Ca-containing alloys are more favorable for basal slip [14]. Thus, the severe stress concentration could be produced, since the dislocation slips are usually blocked at twin boundaries. In order to coordinate the further deformation, the recrystallization is accelerated and the numerous new twins will be formed to provide more space for basal slip. The deformed shear bands are most likely to originate from these intensive new twins. Therefore, the prior formation of the shear bands in AM50−0.3Ca and AM50−0.5Ca alloys can be attributed to the higher proportion of the compression twins. These deformed shear bands consisting of massive deformation twins can effectively facilitate the recrystallization processes, which leads to the more homogeneously-distributed fine recrystallized grains.

3.2 Textures of rolled and annealed alloy sheets

The (0002) pole figures, the texture intensity as a function of the tilt of (0002) plane deviates from ND, and the misorientation angle distributions

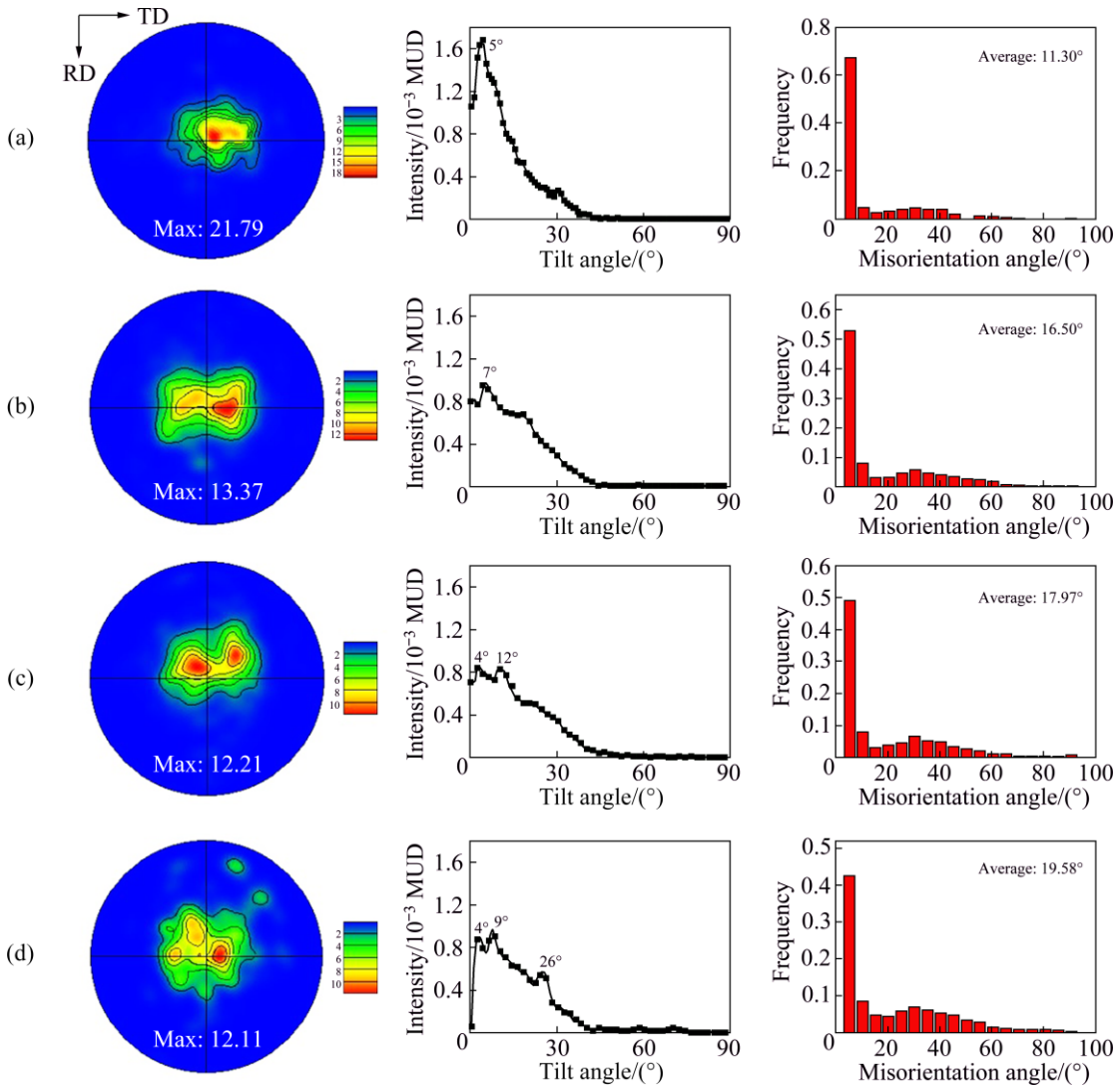

Fig. 2 (0002) pole figures, texture intensity as function of tilt angle of (0002) plane deviations from ND, and misorientation angle distributions of as-rolled alloys at reduction of 87%: (a) AM50; (b) AM50−0.1Ca; (c) AM50−0.3Ca; (d) AM50−0.5Ca

of the as-rolled alloy sheets at the reduction of 87% are shown in Fig. 2. The strong basal texture with a typical characteristic, ⟨0001⟩//ND is observed in AM50 alloy, whereas the weakened basal texture with the slight tilt of basal poles can be found in the case of the Ca-containing alloys. The texture intensity remarkably decreases from 21.79 to 12.11 with the increase of Ca content. It is worth noting that the double-peak texture is apparent in AM50−0.3Ca alloy with the peak intensity points lying at ~4° and ~12°. Similarity, the split of basal pole also appears in the AM50−0.5Ca alloy. It can be seen that the tilt angles of most grains are still within 10°, but there exists a strengthening point at ~26°. The fraction of low-angle grain boundary (LAGB) decreases while that of the high angle grain boundary (HAGB) increases with the increase of Ca addition, which results in the average misorientation angle increasing from 11.30° to 19.58°. The higher content of HAGB in Ca-containing alloys suggests the increased orientations among the grains, indicating the accelerated recrystallization during the deformation process. Therefore, it can be considered that the addition of Ca can effectively promote the recrystallization and thus lead to the basal texture weakening.

During the recrystallization process, the compression twins are the more effective nucleation sites than the tensile twins due to the higher internal storage energy. New grains nucleate at compression twins mainly toward the orientations of the sub-grains, which have been subjected to the complicated orientation rotations [14]. Therefore, the accelerated nucleation at massive compression twins in the initial stage of the deformation is believed to be responsible for the texture weakening. With the increase of the reduction, the recrystallization is intensified and the shear bands become the main nucleation sites of the recrystallized grains. Previous studies have been reported that the shear bands often have basal planes parallel to the shear plane, which usually leads to a wide range of recrystallization orientations [19−21]. This suggests that the split of basal pole in the AM50−0.3Ca and AM50−0.5Ca alloy can be related to the higher proportion of the shear bands.

In addition, the texture weakening is also relevant to the change of the lattice parameters. For the metals with close-packed hexagonal structure, the non-basal slips are more likely to be activated when the alloy has a smaller axial ratio (c/a). It has been studied that the addition of RE element resulted in the decrease of c/a, which contributed to the activation of non-basal slip and then weakened the basal texture [22]. As mentioned above, the radii of Al and Mn atoms are both smaller than the radius of Mg atom while Ca has the larger atomic size with respect to Mg. Therefore, it is suggested that the solid solution of Ca atoms can lead to the lattice distortion and the consequent decrease of c/a ratio. The XRD patterns of four investigated alloys are shown in Fig. 3. The corresponding calculated c/a values are summarized in Table 2. It is observed that compared to the pure Mg, the AM50 alloy exhibits the higher c/a despite the lower a and c values. With the increase of Ca content, the a value increases while the c value decreases, resulting in the c/a ratio decreasing from 1.6245 to 1.6198. This implies that the decrease of c/a also plays an important role in the texture weakening of Ca-containing alloys after the hot rolling.

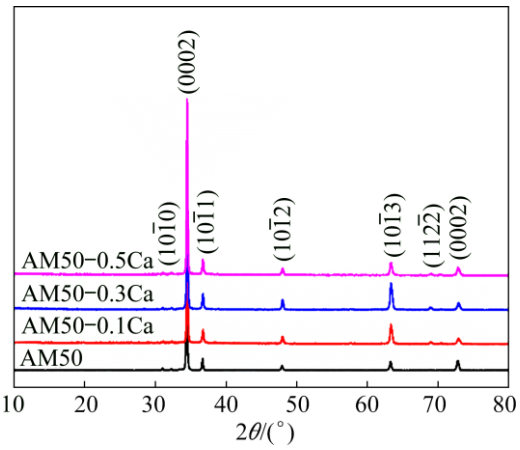

Fig. 3 XRD patterns of alloys for calculation of c/a ratio

Table 2 Lattice parameters and axial ratios of alloys

Specimen	a/nm	c/nm	c/a
Pure Mg	3.2092	5.2105	1.6236
AM50	3.1987	5.1963	1.6245
AM50−0.1Ca	3.2013	5.1935	1.6223
AM50−0.3Ca	3.2026	5.1927	1.6214
AM50−0.5Ca	3.2051	5.1916	1.6198

The orientation maps and (0002) pole figures, as well as the distributions of grain size and

misorientation angle of the annealed alloys are shown in Fig. 4. It can be observed that the average grain size and texture intensity decrease from 12.52 μm to 7.87 μm and from 17.98 to 7.29, respectively, but the average misorientation angle increases from 32.07° to 38.69° with the increase of Ca content. Compared to the alloys in as-rolled condition, the textures of four annealed alloy sheets are further weakened and the fraction of HAGB increases significantly. This suggests that the static recrystallization is promoted during the annealing. In addition, it can be seen that the typical rolling textures are still retained for the AM50 and AM50−0.1Ca alloys, whereas the split of basal poles in AM50−0.3Ca and AM50−0.5Ca alloys are replaced by the single-peak textures with the orientations spreading to TD. As mentioned above, the AM50−0.3Ca and AM50−0.5Ca alloys obtain a portion of deformed structures after the hot rolling. Therefore, the broad spread of the basal planes toward TD can be attributed to the full recrystallization in those fine-grained regions, where the enough storage energy for the nucleation and grain growth can be provided.

3.3 Mechanical properties and stretch formability

The nominal stress−strain curves of the annealed alloy sheets are shown in Fig. 5. Compared to the AM50 alloy, three Ca-containing alloy sheets exhibit the smaller in-plane anisotropy counterpart, which is supported by the closer curves in three tensile directions. The mechanical properties such as the 0.2% proof stress (σ_s), elongation to failure (δ), strain hardening exponent (n-value), and Lankford value (r-value) in the RD, 45° and TD tensile directions, as well as their average values ($\bar{X}=(X_{RD}+2X_{45°}+X_{TD})/4$) are listed in Table 3. It is known from the Hall−Petch formula that the material with smaller average grain size often obtains the higher yield strength. However, the average yield strength decreases from 201 to

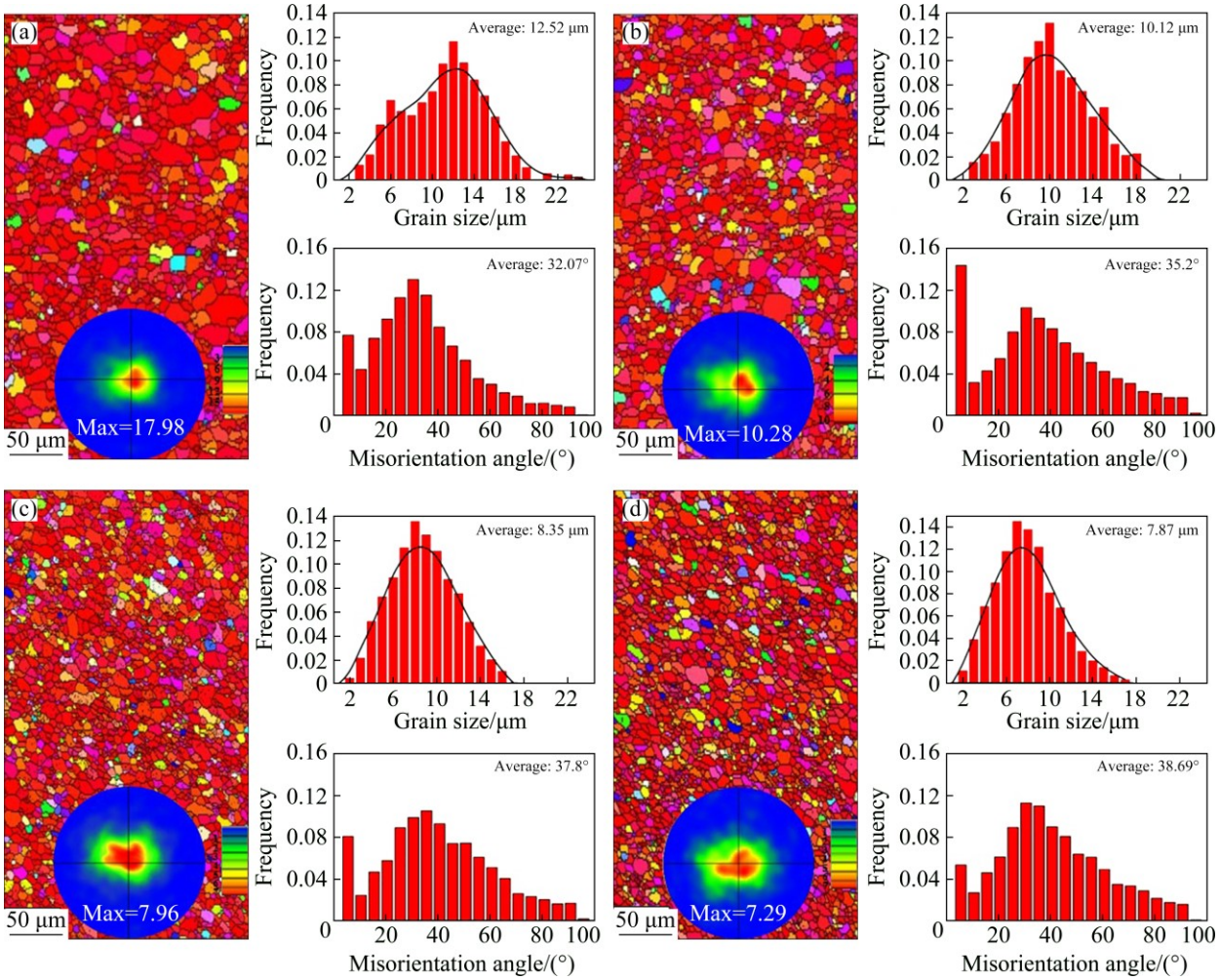

Fig. 4 Orientation maps and (0002) pole figures, as well as distributions of grain size and misorientation angle of annealed alloys: (a) AM50; (b) AM50−0.1Ca; (c) AM50−0.3Ca; (d) AM50−0.5Ca

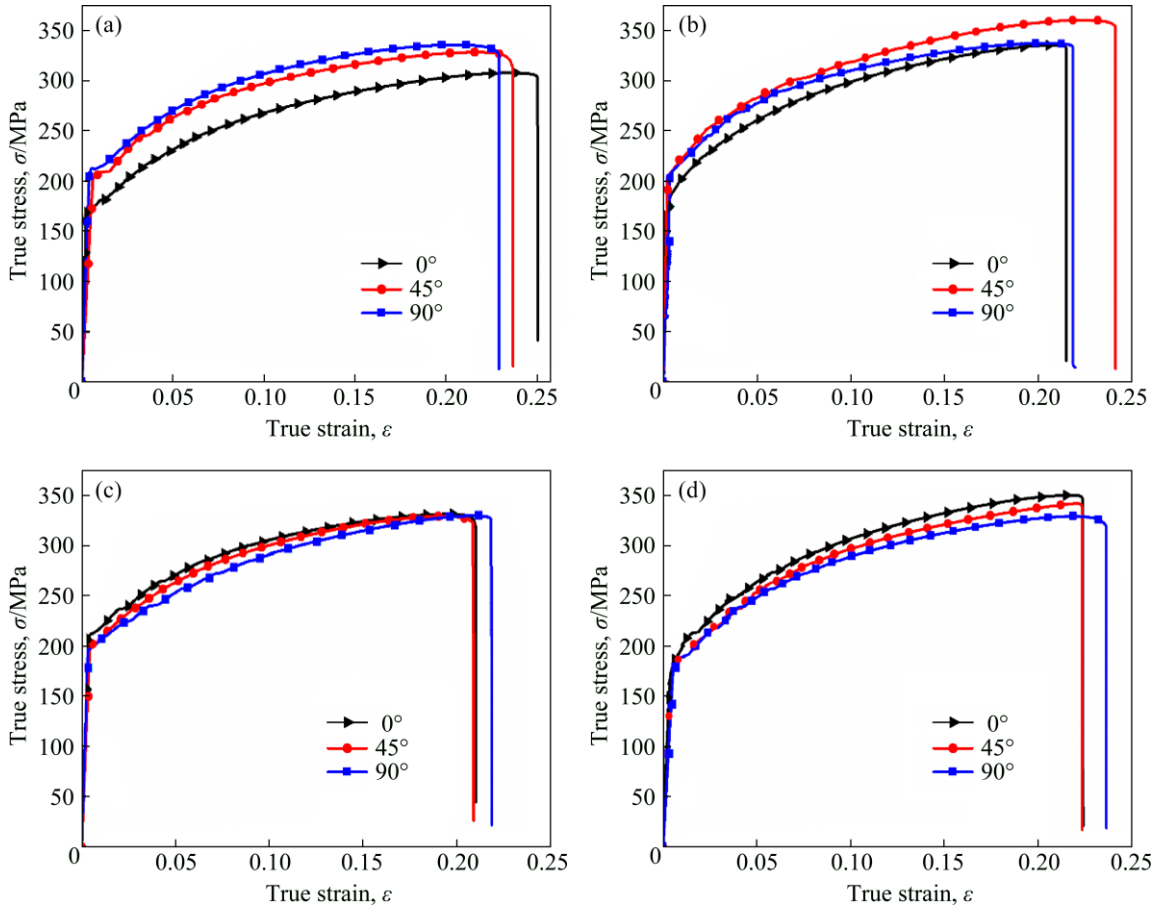

Fig. 5 Nominal stress−strain curves in RD, 45° and TD tensile directions of annealed alloy sheets: (a) AM50; (b) AM50−0.1Ca; (c) AM50−0.3Ca; (d) AM50−0.5Ca

Table 3 Tensile properties in RD, 45° and TD tensile directions of annealed alloy sheets

Alloy	σ_s/MPa			$\bar{\sigma}_s$	δ/MPa			$\bar{\delta}$	n			$\bar{n}$	r			$\bar{r}$
	RD	45°	TD		RD	45°	TD		RD	45°	TD		RD	45°	TD	
AM50	175	208	213	201	25.2	23.7	22.9	23.9	0.20	0.17	0.15	0.17	3.25	3.18	2.78	3.10
AM50−0.1Ca	180	205	203	198	22.4	24.2	22.0	23.2	0.24	0.23	0.21	0.23	2.68	2.56	2.47	2.57
AM50−0.3Ca	190	187	186	187	22.4	21.9	22.8	22.3	0.25	0.24	0.27	0.25	2.52	2.47	2.39	2.46
AM50−0.5Ca	183	179	180	180	21.8	21.4	22.1	21.7	0.26	0.25	0.28	0.26	2.51	2.47	2.40	2.46

180 MPa with the increase of Ca addition in spite of the average grain size decreasing from 12.52 to 7.87 μm. This indicates that the effect of texture weakening plays an important role in the variation of the yield strength. Moreover, the highest σ_s appears in the TD direction in AM50 alloy while the lowest σ_s in this direction is observed in AM50−0.3Ca and AM50−0.5Ca alloys. It can be ascribed to the spread of the (0002) orientation towards TD which is favorable for the basal slip during the tensile deformation.

However, the change of the elongation appears to be relatively insensitive to the weakened basal texture. Specifically, the average elongation decreases from 23.9% to 21.7% with the increase of Ca content. As mentioned above, the addition of Ca has promoted the formation of the shear bands, where numerous deformation twins are concentrated. Currently, the micro-cracks tend to occur in the twin cells or the twin interlaced regions [23,24]. Therefore, the decreased elongation could be ascribed to premature formation of the cracks in extensive twins during the tensile deformation.

The *n*-value reflects the ability of the alloy sheet to resist the uniform plastic deformation. The large *n*-value is known to lead to a reduction in plastic instability, resulting in the enhanced stretch formability. In the present study, the *n*-values in the three tensile directions gradually increase and the average *n*-value increases from 0.17 to 0.26 with the increase of Ca addition. Besides, the largest *n*-values of AM50 and AM50−0.1Ca alloys appear in the RD direction, while the largest *n*-values of AM50−0.3Ca and AM50−0.5Ca alloys are observed in the TD direction. This results from the texture modification. The weakening of basal texture can restrict the softening behavior of the dynamic recovery, which is beneficial to the improvement of the work-hardening ability [25]. For the alloys with 0.3 wt.% and 0.5 wt.% Ca, the basal slip can be facilitated due to the lower texture intensities and the split of basal poles. This contributes to the enhancement of the plastic deformation capacity and therefore results in the larger *n*-value in the TD direction.

The *r*-value is used to evaluate the deep drawability of the alloy sheet. The small *r*-value is beneficial to the sheet thinning which is favorable for the enhancement of stretch formability [26,27]. As shown in Table 3. The *r*-value decreases in the RD and 45° directions whereas the *r*-value decreases firstly and then has a little increase in the TD direction with the increase of Ca content. The average *r*-value decreases from 3.10 to 2.46 and the AM50−0.3Ca and AM50−0.5Ca alloys have the equivalent values. During the in-plane tensile deformation, the width strain and the thickness strain are essentially required due to the fact that the sheet is in a biaxial tensile stress state. It has been reported that the prismatic $\langle a \rangle$ slip always dominates in the width strain, while the thickness strain is usually governed by the pyramidal $\langle c+a \rangle$ slip and twinning [28]. The deformation in the thickness direction of AM50 alloy sheet is difficult to occur due to the strong basal texture, which restricts the pyramidal $\langle c+a \rangle$ slip and twinning, and thus results in the larger *r*-value. However, the TD-inclined basal texture leads to the more complicated grain orientations in the case of Ca-containing alloys. This contributes to the activation of the pyramidal $\langle c+a \rangle$ slip [29]. Moreover, the tilt of basal plane can promote the *c* axis parallel to the tensile direction, which makes it easier to produce the tensile twins during the tensile deformation and therefore results in the decrease of *r*-value.

The change of Erichsen value of the annealed sheets is shown in Fig. 6. With the increase of Ca addition, the average Erichsen value is significantly increased from 2.25 to 4.21 mm by about one times. The enhancement of stretch formability is due to the increase of *n*-value and the decrease of *r*-value, which is attributed to weakened basal texture intensity and split of the basal planes.

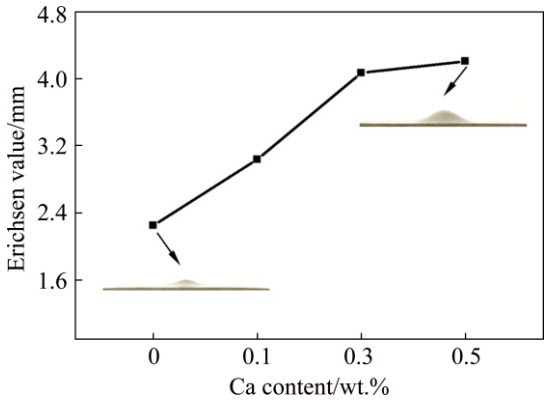

Fig. 6 Erichsen values of annealed alloy sheets and deformed blanks with minimum and maximum values

4 Conclusions

(1) In the early stages of the hot rolling, the addition of Ca facilitates the formation of the compression twins, which gives rise to the appearance of the shear bands.

(2) After the hot rolling, the basal plane deviates from the ND and the texture intensity decreases with the increase of Ca addition. The texture weakening is ascribed to preferential appearance of the compression twins, as well as the decrease of *c*/*a* ratio.

(3) After the annealing, the AM50 and AM50−0.1Ca alloys retain the texture characteristics of the as-rolled condition, whereas the split of basal poles in the AM50−0.3Ca and AM50−0.5Ca alloys are replaced by the single-peak pole with the intensity broadening to TD.

(4) The Erichsen value increases from 2.25 to 4.21 mm with the increase of Ca content. The enhancement of formability is due to the increase of *n*-value and the decrease of *r*-value, which is attributed to the weakened basal texture intensity

and the broad spread of basal poles toward TD.

References

[1] JOOST W J, KRAJEWSKI P E. Towards magnesium alloys for high-volume automotive applications [J]. Scripta Materialia, 2017, 128: 107−112.

[2] PAN Hu-cheng, REN Yu-ping, FU He, ZHAO Hong, WANG Li-qing, MENG Xiang-ying, QIN Gao-wu. Recent developments in rare-earth free wrought magnesium alloys having high strength: A review [J]. Journal of Alloys and Compounds, 2016, 663: 321−331.

[3] YOU Si-hang, HUANG Yuan-ding, KAINER K U, HORT N. Recent research and developments on wrought magnesium alloys [J]. Journal of Magnesium and Alloys, 2017, 5: 239−253.

[4] HUANG Xin-sheng, SUZUKI K, CHINO Y, MABUCHI M. Influence of aluminum content on the texture and sheet formability of AM series magnesium alloys [J]. Materials Science and Engineering A, 2015, 633: 144−153.

[5] DING Han-lin, ZHANG Yi-wei, KAMADO S. Effect of finish-rolling conditions on mechanical properties and texture characteristics of AM50 alloy sheet [J]. Transactions of Nonferrous Metals Society of China, 2014, 24: 2761−2766.

[6] SOMEKAWA H, KINOSHITA A, KATO A. Effect of alloying elements on room temperature stretch formability in Mg alloys [J]. Materials Science and Engineering A, 2018, 732: 21−28.

[7] CAI Zheng-xu, JIANG Hai-tao, TANG Di, MA Zhao, KANG Qiang. Texture and stretch formability of rolled Mg−Zn−RE (Y, Ce, and Gd) alloys at room temperature [J]. Rare Metals, 2013, 32: 441−447.

[8] PARK S J, JUNG H C, SHIN K S. Deformation behaviors of twin roll cast Mg−Zn−X−Ca alloys for enhanced room-temperature formability [J]. Materials Science and Engineering A, 2017, 679: 329−339.

[9] BOHIEN J, WENDT J, NIENABER M, KAINER K U, STUTZ L, LETZIG D. Calcium and zirconium as texture modifiers during rolling and annealing of magnesium-zinc alloys [J]. Materials Characterization, 2015, 101: 144−152.

[10] LEE J Y, YUN Y S, SUH B C, KIM N J, KIM W T, KIM D H. Comparison of static recrystallization behavior in hot rolled Mg−3Al−1Zn and Mg−3Zn−0.5Ca sheets [J]. Journal of Alloys and Compounds, 2014, 589: 240−246.

[11] DING Han-lin, ZHANG Peng, CHENG Guang-ping, KAMADO S. Effect of calcium addition on microstructure and texture modification of Mg rolled sheets [J]. Transactions of Nonferrous Metal Society of China, 2015, 25: 2875−2883.

[12] DING Han-lin, SHI Xiao-bin, WANG Yong-qiang, CHENG Guang-ping, KAMADO S. Texture weakening and ductility variation of Mg−2Zn alloy with CA or RE addition [J]. Materials Science and Engineering A, 2015, 645: 196−204.

[13] LASER T, HARTIG C, NÜRNBERG M R, LETZIG D, BORMANN R. The influence of calcium and cerium mischmetal on the microstructural evolution of Mg−3Al−1Zn during extrusion and resulting mechanical properties [J]. Acta Materialia, 2008, 56: 2791−2798.

[14] LI Xiao, YANG Ping, WANG Li-na, MENG Li, CUI Feng-e. Orientational analysis of static recrystallization at compression twins in a magnesium alloy AZ31 [J]. Materials Science and Engineering A, 2009, 517(1−2): 160−169.

[15] LI Xiao, YANG Ping, MENG Li, CUI Feng-e. Analysis of the static recrystallization at tension twins in AZ31 magnesium alloy [J]. Acta Metallurgica Sinica, 2010, 46(2): 147−154. (in Chinese)

[16] REED-HILL R E, ROBERTSON W D. Additional modes of deformation twinning in magnesium [J]. Acta Metallurgica, 1957, 5: 717−727.

[17] SANDlŐBES S, FRIÁK M, ZAEFFERER S, DICK A, YI S, LETZIG D, PEI Z, ZHU L, NEUGEBAUER J, RAABE D. The relation between ductility and stacking fault energies in Mg and Mg−Y alloys [J]. Acta Materialia, 2012, 60: 3011−3021.

[18] WANG Cheng, ZHANG Hua-yuan, WANG Hui-yuan, LIU Guo-jun, JIANG Qi-chuan. Effects of doping atoms on the generalized stacking-fault energies of Mg alloys from first-principles calculations [J]. Scripta Materialia, 2013, 69: 445−448.

[19] SANDLŐBES S, ZAEFFERER S, SCHESTAKOW I, YI S, GONZALEZ-MARTINEZ R. On the role of non-basal deformation mechanisms for the ductility of Mg and Mg−Y alloys [J]. Acta Materialia, 2011, 59: 429−439.

[20] BASU I, AL-SAMMAN T, GOTTSTEIN G. Shear band-related recrystallization and grain growth in two rolled magnesium-rare earth alloys [J]. Materials Science and Engineering A, 2013, 579: 50−56.

[21] IMANDOUST A, BARRETT C D, OPPEDAL A L, WHITTINGTON W R, PAUDEL Y, KADIRI H E. Nucleation and preferential growth mechanism of recrystallization texture in high purity binary magnesium-rare earth alloys [J]. Acta Materialia, 2017, 138: 27−41.

[22] BOHLEN J, NÜRNBERG M R, SENN J W, LETZIG D, AGNEW S R. The texture and anisotropy of magnesium−zinc−rare earth alloy sheets [J]. Acta Materialia, 2007, 55: 2101−2112.

[23] WANG Bao-jie, XU Dao-kui, WANG Shi-dong, SHENG Li-yuan, ZENG Rong-chang, HAN En-hou. Influence of solution treatment on the corrosion fatigue behavior of an as-forged Mg−Zn−Y−Zr alloy [J]. International Journal of Fatigue, 2019, 120: 46−55.

[24] WANG Bao-jie, XU Dao-kui, WANG Shi-dong, HAN En-hou. Fatigue crack initiation of magnesium alloys under elastic stress amplitudes: A review [J]. Frontiers of Mechanical Engineering, 2019, 14(1): 113−127.

[25] HUANG Xin-sheng, SUZUKI K, WATAZU A, SHIGEMATSU I, SAITO N. Mechanical properties of Mg−Al−Zn alloy with a tilted basal texture obtained by differential speed rolling [J]. Materials Science and Engineering A, 2008, 488: 214−220.

[26] CHAUDRY U M, KIM Y S, HAMAD K. Effect of Ca addition on the room-temperature formability of AZ31 magnesium alloy [J]. Materials Letters, 2019, 238: 305−308.

[27] HUANG Xin-sheng, SUZUKI K, CHINO Y, MABUCHI M. Texture and stretch formability of AZ61 and AM60

magnesium alloy sheets processed by high-temperature rolling [J]. Journal of Alloys and Compounds, 2015, 632: 94−102.
[28] KOIKE J. Geometrical criterion for the activation of prismatic slip in AZ61 Mg alloy sheets deformed at room temperature [J]. Acta Materialia, 2005, 53: 1963−1972.
[29] WANG Jing, ZHANG Xin-jian, LU Xi, YANG Yuan-sheng, WANG Zhen-hong. Microstructure, texture and mechanical properties of hot-rolled Mg−4Al−2Sn−0.5Y−0.4Nd alloy [J]. Journal of Magnesium and Alloys, 2016, 4: 207−213.

微量 Ca 添加对 AM50 镁合金板材织构及成形性能的影响

赵红亮[1]，华云筱[1]，董祥雷[1]，邢 辉[2]，卢艳丽[3]

1. 郑州大学 材料科学与工程学院，郑州 450001；
2. 西北工业大学 超常条件材料物理与化学教育部重点实验室，西安 710129；
3. 西北工业大学 凝固技术国家重点实验室，西安 710072

摘 要：为研究微量 Ca 添加对 AM50 镁合金织构及成形性能的影响，对 AM50、AM50−0.1Ca、AM50−0.3Ca 和 AM50−0.5Ca(质量分数，%) 4 种合金进行热轧，并对其力学性能进行测试。结果表明，微量 Ca 添加有效改善基面织构：热轧后合金基极偏离法向(ND)，退火后基面向横向(TD)延伸。织构的改变与大量压缩孪晶的优先形成以及 *c*/*a* 值的减小有关。随 Ca 含量增加，合金杯突值由 2.25 升高至 4.21 mm，其成形性能的提高归因于基面织构的弱化导致 *n* 值增加和 *r* 值减小。

关键词：镁合金；Ca 添加；织构；成形性能；力学性能

(Edited by Bing YANG)